APS physics

CHORUS

This is the accepted manuscript made available via CHORUS. The article has been published as:

Precision Control of the Electron Longitudinal Bunch Shape Using an Emittance-Exchange Beam Line

G. Ha, M. H. Cho, W. Namkung, J. G. Power, D. S. Doran, E. E. Wisniewski, M. Conde, W. Gai, W. Liu, C. Whiteford, Q. Gao, K.-J. Kim, A. Zholents, Y.-E Sun, C. Jing, and P. Piot

Phys. Rev. Lett. **118**, 104801 — Published 9 March 2017

DOI: 10.1103/PhysRevLett.118.104801

Precision control of the longitudinal electron bunch shape using an emittance exchange beamline

G. Ha*, M. H. Cho, and W. Namkung

POSTECH, Pohang, Gyeongbuk 37673, Republic of KOREA

J. G. Power, D. S. Doran, E. E. Wisniewski, M. Conde, W. Gai, W. Liu, C. Whiteford. Q. Gao, K. –J. Kim, A. Zholents, and Y. –E Sun

Argonne National Laboratory, Argonne, IL 60439, USA

C. Jing

Euclid TechLabs, Solon, Ohio 44139, USA

P. Piot

Fermi National Accelerator Laboratory, Batavia, IL 60510, USA

We report on the experimental generation of relativistic electron bunches with tunable longitudinal bunch shape. A longitudinal bunch shaping (LBS) beamline, consisting of a transverse mask followed by a transverse-to-longitudinal emittance exchange (EEX) beamline, is used to tailor the longitudinal bunch shape (or current profile) of the electron bunch. The mask shapes the bunch's horizontal profile and the EEX beamline converts it to a corresponding longitudinal profile. The Argonne Wakefield Accelerator RF photoinjector delivered electron bunches into a LBS beamline to generate a variety of longitudinal bunch shapes. The quality of the longitudinal bunch shape was limited by various perturbations in the exchange process. We have developed a simple method, based on the incident slope of the bunch, to significantly suppress the perturbations.

Precise methods to manipulate the 6-dimensional (6D) phase space of high-brightness, relativistic electron bunches are attracting increasing attention. This interest is being driven by the awareness that the next generation of electron linear accelerator applications (e.g. a future linear collider or X-ray light sources [1-3]) will demand unprecedented control over both the beam's transverse and longitudinal phase space.

Manipulation in transverse phase space is straightforward through the use of multipole magnets (e.g. quadrupoles), collimators, etc. Longitudinal phase space manipulation is considerably more difficult to achieve. While it is straightforward to manipulate the momentum with an accelerating cavity, the longitudinal distribution of particles within the bunch is difficult to control due to the short duration of the typical high-brightness electron bunch (sub-picosecond to tens of picosecond scale). Thus, longitudinal bunch shaping has remained elusive until the last decade where a few different methods have been suggested [4-10].

There are many electron linac based applications that would benefit from precisely tailored longitudinal bunch shapes. These include, superradiant radiation [11-13], beam quality control for high brightness beam [14-18], seeding techniques to enhance the performances of X-ray free electron laser [19-21], and improving efficiency of ultra-high gradient wakefield accelerations [22-24].

Longitudinal bunch shaping has become an active area of R&D in recent years due, in part, to the recent progress in accurate simulations and precise experimental methods. There are two fundamental approaches that can be taken to manipulate the longitudinal bunch shape: correlation-based and exchange-based methods. The former method introduces a temporary correlation between the longitudinal position (z) and another coordinate which is easier to control [e.g. the horizontal position (x) or the fractional momentum deviation (δ)]. Once the correlation is established, the bunch distribution is manipulated along the other coordinate (e.g. by using a collimator) and the correlation is finally removed. Thus, these approaches indirectly control the longitudinal distribution by manipulating another coordinate as exemplified in Ref. [4,5].

In this Letter, we present the first experimental demonstration of an alternative bunch-shaping technique based on a phase-space exchange scheme [6] that employs a transverse-to-longitudinal emittance exchange (EEX) beamline [1,25,26]. Instead of introducing a correlation between z and another axis (x or δ), this method exchanges the horizontal phase space coordinates (x, x') with the longitudinal phase space ones (z, δ), where x' is the horizontal angle. Consequently, any features introduced in the horizontal phase space can be transferred to the longitudinal phase space. The advantage of this method is that the mature techniques of transverse phase space manipulation can be used to control the longitudinal bunch shape. Thus, in principle, the exchange-based method is capable of realizing arbitrary control over the longitudinal bunch shape [6].

The longitudinal bunch-shaping method used in the experiment incorporated a transverse intercepting mask located about 1 meter upstream of the EEX beamline.

There are several different beamline configurations [27,28] that can exchange the horizontal and longitudinal emittance, as long as the beamline satisfies the general EEX condition [29]. We used the double dogleg EEX beamline since it has the simplest form making it an ideal candidate for understanding the fundamental beam dynamics of the bunch shaping process. The double dogleg EEX beamline consists of two identical doglegs each with dispersion η, and a transverse deflecting cavity (TDC), of normalized kick strength κ where $\kappa = \frac{eV}{pc}\frac{2\pi}{\lambda}$ (e is the electronic charge, pc is the mean momentum, V is the deflecting voltage, and λ is the RF wavelength), in between the doglegs (FIG. 1). For this beamline, the EEX condition is $1 + \kappa\eta = 0$. This is the condition that produces the zero-diagonal elements in the transfer matrix for (x, x', z, δ) phase space [1]. The exchange process can be fully described in 4D phase space via the linear transfer matrix

$$\begin{pmatrix} x_f \\ x'_f \\ z_f \\ \delta_f \end{pmatrix} = \begin{pmatrix} 0 & 0 & \kappa(L+L_D) & \eta + \kappa\xi(L+L_D) \\ 0 & 0 & \kappa & \kappa\xi \\ \kappa\xi & \eta + \kappa\xi(L+L_D) & 0 & 0 \\ \kappa & \kappa(L+L_D) & 0 & 0 \end{pmatrix} \begin{pmatrix} x_i \\ x'_i \\ z_i \\ \delta_i \end{pmatrix}, \quad (1)$$

where $L = 2L_B/\cos(\alpha) + L_{DL}/\cos^2(\alpha)$, $\eta = 2L_B(\cos(\alpha) - 1)/\sin(\alpha)\cos(\alpha) - L_{DL}\sin(\alpha)/\cos^2(\alpha)$, $\xi = L_{DL}\sin^2(\alpha)/\cos^2(\alpha) + 2L_B/\cos(\alpha) - 2L_B\alpha/\sin(\alpha)$, L_B is the length of dipole, α is the bending angle, L_{DL} is the length between dipoles (B-to-B), and L_D is the length between dipole and TDC [31]. In this equation we used rectangular dipole magnets and the thin-lens approximation of the TDC to calculate the transfer matrix.

Since the anti-diagonal 2x2 blocks in the transfer matrix are zero, the final longitudinal coordinates (z_f, δ_f) solely depend on the incoming horizontal coordinates (x_i, x'_i) and vice versa.

Additionally, by properly tuning the incoming phase space correlations, e.g. in the (x_i, x'_i) phase space, the relationship between z_f and x_i can be further simplified to,

$$z_f = \{\kappa\xi + S(\eta + \kappa\xi(L + L_D))\}x_i, \quad (2)$$

where $S \equiv dx/dx'|_{x=0}$ is the slope of initial phase space [32] and κ and η satisfy the EEX condition. According to Eq. (2), any initial horizontal density profile can be mapped to the final longitudinal density profile. A transverse mask was used to tailor the horizontal profile due to its simplicity. Given the interceptive nature of such a mask, the implementation of the proposed bunch shaping technique in high-energy or high-repetition accelerators, would have to be performed at low energies where beam losses can be tolerated.

The longitudinal bunch shaping experiment was performed at the Argonne Wakefield Accelerator (AWA) facility [33] and is diagrammed in FIG. 1. It consists of the following four sections: (1) the RF photoinjector, (2) the transverse manipulation beamline, (3) the EEX beamline, and (4) the main diagnostic beamline.

In the L-band 1.5 cell RF photoinjector, a 5-nC, 8-MeV electron bunch was generated and further accelerated through the linear accelerator (linac) to a final energy of 48 MeV. The electron bunch phase is normally set to on-crest (0 degree) in the cavities, but can be adjusted in order to control the longitudinal slope (i.e. chirp). (A negative phase reduces the energy of the head and increases the energy of the tail.)

The transverse manipulation beamline included four quadrupole magnets and a series of selectable 100 micron thick tungsten masks. The quadrupole magnets controlled the size and slope of the horizontal and vertical phase ellipse. Each transverse mask generated a different initial horizontal profile [34] by scattering the unwanted portion of the beam. The initial horizontal bunch profile was measured with a YAG screen located in the straight ahead line (YAG1).

The EEX beamline used rectangular dipole magnets (B) to bend the electron bunch by 20 degrees. Each dogleg generated a horizontal dispersion of $\eta_x \cong 0.9$ m and a momentum compaction factor of $\xi \cong 0.3$ m [35]. The L-band TDC in the middle of EEX beamline (TDC1) consists of 3 cells [36]. The power applied to the TDC1 was adjusted to satisfy the EEX condition $1 + \kappa\eta = 0$.

In the main diagnostic beamline, located after the EEX beamline, three quadrupole magnets and a TDC were installed along with YAG screens both upstream (YAG2) and downstream (YAG3) of TDC2. During its nominal operation (5 MW input power), TDC2 can resolve the bunch longitudinal profile with a resolution of less than 30 μm.

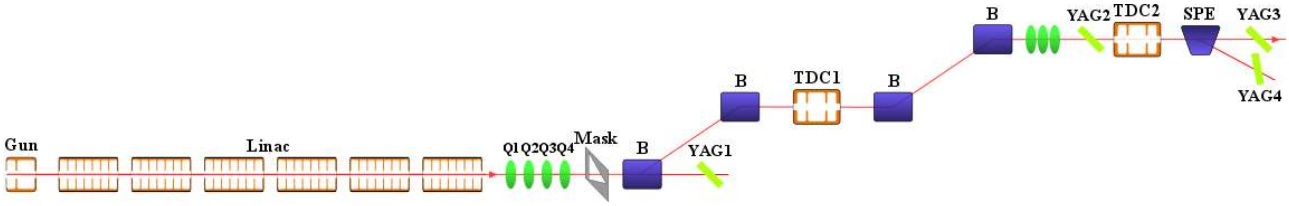

FIG. 1. Schematic diagram of the experimental beam. The acronyms Q, B, TDC and SPE stand for the quadrupole magnet, dipole magnet, transverse deflecting cavity and spectrometer respectively. Dipole magnets and TDC1 bend or kick the beam horizontally, and TDC2 kicks the beam vertically.

The first set of experiments focused on demonstrating the longitudinal bunch shaping capabilities of the exchange-based method (see FIG. 2). The top row of FIG. 2 shows transverse bunch images at YAG1 without mask (a) and with several different masks (b-e). The total charge before the mask was ~5 nC which was reduced after the mask to ~1-1.5 nC depending on the mask used. The electron bunch had an approximately symmetric horizontal profile before the mask (a), and was converted into two rectangular-shaped transverse beamlets (b), a triangle (c), a rectangle (d) and a trapezoid (e). These transversely shaped electron bunches were transported through the EEX beamline and their final longitudinal density profiles were measured with TDC2 at YAG3.

The bottom row of FIG. 2 shows the longitudinal bunch shapes measured at YAG3 (g-j) that corresponds to the horizontal bunch shapes in the top row. Note that the longitudinal bunch shape in (f) corresponds to the horizontal bunch without a mask in (a). As can be seen, the final longitudinal bunch shapes closely follow the corresponding initial horizontal bunch shapes. We observe a longitudinally separated 2-bunch train (g), a triangle (h), a rectangle (i) and a trapezoid (j).

The bottom row of FIG. 2 also shows the final horizontal distribution of the bunch which is determined by its initial longitudinal features. The final horizontal bunch shapes in FIG. 2 (f-j) retain none of their initial horizontal shape from the mask. Instead, all of the horizontal distributions show a similar asymmetric pattern, brighter on the top and dimmer on the bottom, due to a weak transverse-longitudinal correlation before the mask. The slight difference in the asymmetric patterns between (g-h) is because the different masks cut the initial profiles in different ways.

While this letter is focused on the final longitudinal bunch shape, we note that all of the other final beam properties at the exit of the EEX beamline can be controlled. Final transverse properties are controlled with quadrupoles after the EEX beamline and final longitudinal properties can be controlled with quadrupoles between the mask and the first EEX dipole. An experiment is planned that will use this beamline to create a drive and witness beam and make them pass through a dielectric structure with a small aperture to achieve high transformer ratio [37]. The only limitation of this beamline is that the final horizontal emittance is large (due to the initial longitudinal emittance) but this can be overcome with a double EEX beamline [14].

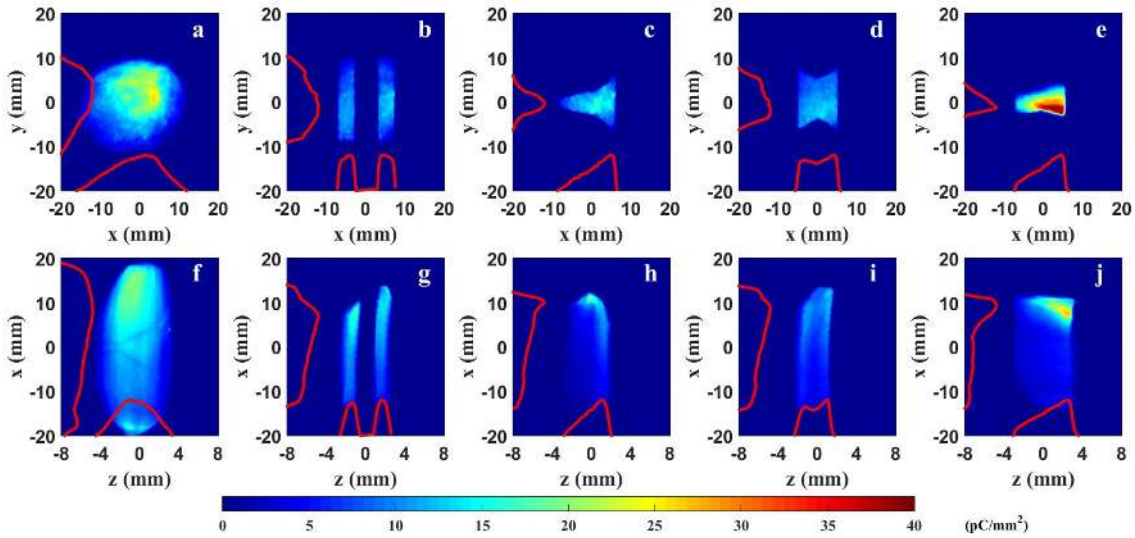

FIG. 2. Electron beam images at YAG1 with different masks (a-e) and corresponding beam images at YAG3 with TDC2 on. The x-axis of the images f-j is rescaled based on the TDC2 calibration. The red traces are the corresponding projections.

The second experimental result we present is the first demonstration of a new perturbation suppression method that we term the slope-control method. We begin this section of the paper by discussing the perturbations observed during the experiment, next we describe the method used to suppress the perturbations, and finally, present the results.

Equations 1 and 2 imply perfect conversion from the horizontal to the longitudinal shape. In reality, these equations ignore important perturbations including: finite bunch emittance, the thick-lens effect of the TDC, second-order effects and collective effects [38,39]. These perturbations distort the ideal longitudinal bunch shape as can be clearly seen by comparing FIG. 2 (b) and (g). Each horizontal beamlet produced by the 2-slit mask has a sharp, rectangle-like shape (FIG. 2b). According to Eq. 1 and 2, the longitudinal bunch train should have the same rectangular shape but the sharp features of the profile are smeared (FIG. 2g) due to the aforementioned perturbations.

Previous researchers have studied several different types of linear perturbations that arise in the EEX beamline and have proposed several methods to suppress them [14,25,39]. In our previous theoretical work [30], we derived analytic expressions for both linear and nonlinear

perturbations and, further, we developed a new method to suppress them termed the "slope-control method".

The slope-control method adjusts the three incoming slopes, in the x, y, and z phase spaces, to partially suppress the perturbations due to the linear thick-lens effect as well as the nonlinear effects: horizontal second-order terms, vertical second-order terms, and longitudinal sources including second-order terms, and collective effects due to space-charge (SC) and coherent synchrotron radiation (CSR). As an example, the perturbation due to the horizontal second order terms was shown in Ref. [30] to be given by the expression: $\Delta z_f \approx A\langle x_0^2\rangle + B\langle x_0 x_0'\rangle + C\langle x_0'^2\rangle$. This perturbation can be minimized by taking the partial derivative of it with respect the slope of the incident bunch ($\langle x_i x_i'\rangle/\langle x_i^2\rangle$) in which case the minimizing slope before the mask is $-A/2C$. In general, the slope-control method is powerful and simple since it can suppress nonlinear perturbations and does not require any significant modification to the beamline. In our experiment, the bunch length was ~10 ps and the slope-control method worked well for our range of parameters.

During the experiment, the linac (FIG. 1) phase was used to control the longitudinal slope (i.e. chirp) and the four quadrupole (Q1-Q4 in FIG. 1) in front of EEX beamline were used to control both the horizontal and vertical bunch sizes and slopes at the mask.

To demonstrate the perturbation suppression method, the longitudinal bunch shape was monitored while the three slopes were varied. The optimal values of the slopes are defined as the values of slopes chosen to suppress the perturbations. The optimal values were calculated [30] to be -0.27 m^{-1} for the horizontal, 0.13 m^{-1} for vertical, and linac phase of -15 degree. During the experiment, the values of the slopes were varied about the base values that we define as 0.0 m^{-1} for the horizontal and vertical slopes and a linac phase of -15 degree, since these are the values the RF photoinjector is typically operated and it is hard to sustain the transverse slope exactly at the optimal values with different RF phases.

The experimental values of the transverse slopes were calculated from the measurement of the beam sizes at the mask position (YAG screen not shown) and YAG1 (FIG. 1). This value is an approximation of the conventional slope and therefore has a small error [32]. The experimental value of the longitudinal chirp was inferred from the linac phase measurement.

During the experiment, one slope was varied at a time while the other two slopes were held constant at their base values while the final longitudinal bunch shape was monitored. FIG. 3 shows the experimental data of the initial horizontal profile measured at YAG1 (blue) and the final longitudinal profile measured at YAG3 (red) for different transverse slopes and linac phase settings. The horizontal profile is scaled using the transfer matrix to convert it ideal longitudinal profile. Ideally these profiles would be identical.

The effect of the horizontal slope on perturbation suppression is shown in the top row of FIG. 3. The four profiles (a-d) correspond to incoming horizontal slopes of $\{0.0, +0.2, +0.4, +0.6\}$ m^{-1}. Note that for the slopes of both 0.0 m^{-1} and +0.2 m^{-1}, the initial horizontal profile and final longitudinal profile show good agreement. However, the head (right side) of the beam has a convex curvature as the horizontal slope increases while the tail length, from the peak to the left end of the profile, stays approximately 1 mm. This is in good agreement with the analytically predicted of the slope needed to suppression the perturbations [30].

With the horizontal slope fixed at 0.0 m^{-1}, the effect of the vertical slope on perturbation suppression is shown in the middle row of FIG. 3. The four profiles (e-h) correspond to the incoming vertical slopes of $\{-0.6, 0.0, +0.2, +0.6\}$ m^{-1}. Again, both 0.0 m^{-1} and +0.2 m^{-1} cases show good agreement between the initial and final profiles. Each extreme slope case shows significant perturbations in which electrons are shifted towards the head or the tail. This perturbation pattern also shows reasonable agreement with the analytically predicted pattern from the vertical second-order terms given in [30].

The effect of the longitudinal chirp on the perturbation suppression is shown in the last row of FIG. 3 and is more complicated than the transverse slopes. This is because the chirp controls three limiting factors at the same time. The thick-length effect and the second-order beam dynamics can be minimized with the longitudinal chirp of $-1/\xi$ [25,30]. Unfortunately, this chirp also minimizes the bunch length before the second dogleg so it results in a strong SC or CSR effect on the shaped longitudinal profile [38]. The four profiles (i-l) correspond to the linac phase of $\{-10°, -15°, -25°, -40°\}$. Compared with the base phase, $-15°$, the phase $-10°$ generates a longer tail while the head of the profile still has a reasonable agreement with the initial profile. Because of the single triangle profile, the perturbation from the thick-lens effect mostly changes the tail length. However, the $-25°$ case makes a longer tail and changes the head simultaneously. In this case, CSR dominates the perturbation on the profile. Thus, it makes overall bunch length longer than expected. The same patterns become even clearer at $-40°$.

Overall, the measurements (FIG. 3) are in reasonable agreement with the predicted slopes.

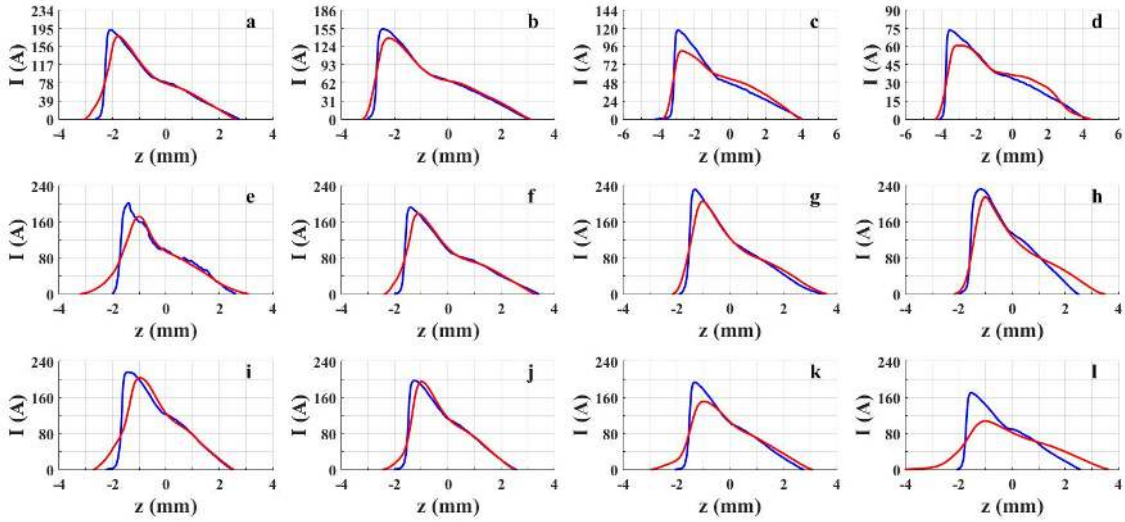

FIG. 3. Horizontal density profiles measured at YAG1 with the first EEX dipole off (blue) and longitudinal density profiles measured at YAG3 with TDC2 on (red). Base line for horizontal and vertical slopes were zero, and linac phase was -15 degree. Each setting was fixed to base line while one of them was scanned. Horizontal slopes of the incoming electron beam were 0.0 m^{-1}, 0.2 m^{-1}, 0.4 m^{-1}, and 0.6 m^{-1} for (a-d). Vertical slopes were -0.6 m^{-1}, 0.0 m^{-1}, 0.2 m^{-1}, and 0.6 m^{-1} for (e-h). Linac phase which control the longitudinal chirp was -10 deg, -15 deg, -25 deg, and -40 deg for (i-l). Here the tail of the profile indicates the peak to the left end of the profile.

In summary, we experimentally demonstrated the ability of the phase-space-exchange method to form arbitrarily-shaped longitudinal profiles. We also validated a simple aberration-control scheme that circumvents possible limitations of the technique. These experimental results confirms the power and versatility of the phase-space exchange based shaping technique and should prove useful to advance beam-driven acceleration techniques, accelerator-based light sources and a wide range of future electron linac applications.

Acknowledgement

This work is supported by POSTECH and Department of Energy, Office of High Energy Physics, under Contract No. DE-AC02-06CH11357.

Reference

[1] P. Emma, Z. Huang, K. –J. Kim, and P. Piot, Phys. Rev. ST Accel. Beams **9**, 100702 (2006).
[2] R. Brinkmann, Y. Derbenev, and K. Flottmann, Phys. Rev. ST Accel. Beams **4**, 053501 (2001).
[3] C. Feng, T. Zhang, H. Deng, and Z. Zhao, Phys. Rev. ST Accel. Beams **17**, 070701 (2014).
[4] P. Muggli et al., Phys. Rev. ST Accel. Beams **13**, 052803 (2010).
[5] P. Piot et al., Phys. Rev. Lett. **108**, 034801 (2012).
[6] P. Piot, Y. –E Sun, J. G. Power, and M. Rihaoui, Phys. Rev. ST Accel. Beams **14**, 022801 (2011).
[7] R. J. England, J. B. Rosenzweig, and G. Travish, Phys. Rev. Lett. **100**, 214802 (2008).
[8] F. Lemery and P. Piot, Phys. Rev. ST Accel. Beams **18**, 081301 (2015).
[9] C. Jing *et al.*, Phys. Rev. ST Accel. Beams **14**, 021302 (2011).
[10] G. Penco et al., Phys. Rev. Lett. **112**, 044801 (2014).
[11] A. Halperin, A. Gover, and A. Yariv, Phys. Rev. A **50**, 4 (1994).
[12] S. E. Korbly, A. S. Kesar, J. R. Sirigiri, and R. J. Temkin, Phys. Rev. Lett. **94**, 054803 (2005).
[13] S. Antipov et al., Phys. Rev. Lett. **111**, 134802 (2013).
[14] A. A. Zholents and M. S. Zolotorev, ANL-APS-LS-327, (2011).
[15] B. E. Carlsten, K. A. Bishofberger, S. J. Russell, and N. A. Yampolsky, Phys. Rev. ST Accel. Beams **14**, 084403 (2011).
[16] S. Antipov et al., Phys. Rev. Lett. **112**, 114801 (2014).
[17] A. Zholents et al., Nucl. Instrum. Methods Phys. Res., Sect. A **829**, 190 (2016).
[18] C. Mitchell, J. Qiang, and P. Emma, Phys. Rev. ST Accel. Beams **16**, 060703 (2013).
[19] L. –H. Yu et al., Science **289**, 932 (2000).
[20] D. Xiang and G. Stupakov, Phys. Rev. ST Accel. Beams **12**, 030702 (2009).
[21] B. Jiang, J. G. Power, R. Lindberg, W. Liu, and W. Gai, Phys. Rev. Lett. **106**, 114801 (2011).
[22] C. Jing et al., Phys. Rev. Lett. **98**, 144801 (2007).
[23] B. Jiang, C. Jing, P. Schoessow, J. Power, and W. Gai, Phys. Rev. ST Accel. Beams **15**, 011301 (2012).
[24] M. Tzoufras et al., Phys. Rev. Lett. **101**, 145002 (2008).
[25] M. Cornacchia and P. Emma, Phys. Rev. ST Accel. Beams **5**, 084001 (2002).
[26] Y. –E Sun et al., Phys. Rev. Lett. **105**, 234801 (2010).
[27] D. Xiang and A. Chao, Phys. Rev. ST Accel. Beams **14**, 114001 (2011).
[28] C. R. Prokop et al., in Proceedings of the 2013 International Particle Accelerator Conference, Shanghai, China (2013), p. 3103.
[29] R. P. Fliller III, Fermi Beams-doc-2553, (2006).
[30] G. Ha et al., unpublished yet.

[31] Y. –E Sun et al., in Proceedings of the 2007 Particle Accelerator Conference, Albuquerque, New Maxico, USA (2007), p. 3441.
[32] A. W. Chao, K. H. Mess, M. Tigner, and F. Zimmermann, "Handbook of Accelerator Physics and Engineering", (World Scientific, 2013).
[33] M. Conde et al., in Proceedings of the 2015 Particle Accelerator Conference, Richmond, VA, USA (2015), p. 2472.
[34] J. G. Power et al., in Proceedings of the 2014 International Particle Accelerator Conference, Dresden, Germany (2014), p. 1506.
[35] G. Ha et al., in Proceedings of the 2015 International Particle Accelerator Conference, Richmond, VA, USA (2015), p. 2575.
[36] M. Conde et al., in Proceedings of the 2012 International Particle Accelerator Conference, New Orleans, Louisiana, USA (2012), p. 3350.
[37] Q. Gao et al., in Proceedings of the 2016 North America Particle Accelerator Conference, Chicago, IL, USA (2016), THPOA08.
[38] G. Ha et al., AIP Conf. Proc. **1507**, 693 (2012).
[39] D. Y. Shchegolkov and E. I. Simakov, Phys. Rev. ST Accel. Beams **17**, 041301 (2014).